

## Original Research

## FBXL6 depletion restrains clear cell renal cell carcinoma progression

Yongchun Yu<sup>a</sup>, Wenhao Yao<sup>a</sup>, Tengda Wang<sup>a</sup>, Wei Xue<sup>a</sup>, Yuyang Meng<sup>a</sup>, Licheng Cai<sup>a</sup>, Wengang Jian<sup>a</sup>, Yipeng Yu<sup>a</sup>, Cheng Zhang<sup>a,b,\*</sup><sup>a</sup> Department of Urology, The First Affiliated Hospital of Harbin Medical University, Harbin, 150001, China<sup>b</sup> School of Medicine, Zhejiang University, Hangzhou, 310058, China

## ARTICLE INFO

## Keywords:

Clear cell renal cell carcinoma  
F-box protein  
Prognostic model  
FBXL6  
SP1

## ABSTRACT

**Background:** F-box proteins play important roles in cell cycle and tumorigenesis. However, its prognostic value and molecular function in clear cell renal cell carcinoma (ccRCC) remain unclear. In this study, we established a survival model to evaluate the prognosis of patients with ccRCC using the F-box gene signature and investigated the function of FBXL6 in ccRCC.

**Methods:** Comprehensive bioinformatics analyses were used to identify differentially expressed F-box and hub genes associated with ccRCC carcinogenesis. Based on the F-box gene signature, we constructed a risk model and nomogram to predict the overall survival (OS) of patients with ccRCC and assist clinicians in decision-making. Finally, we verified the function and underlying molecular mechanisms of FBXL6 in ccRCC using CCK-8 and EdU assays, flow cytometry, and subcutaneous xenografts.

**Results:** A risk model based on FBXO39, FBXL6, FBXO1, and FBXL16 was developed. In addition, we drew a nomogram based on the risk score and clinical features to assess the prognosis of patients with ccRCC. Subsequently, we identified FBXL6 as an independent prognostic marker that was highly expressed in ccRCC cell lines. In vivo and in vitro assays revealed that the depletion of FBXL6 inhibited cell proliferation and induced apoptosis. We also demonstrated that SP1 regulated the expression of FBXL6.

**Conclusions:** FBXL6 was first identified as a diagnostic and prognostic marker in patients with ccRCC. Loss of FBXL6 attenuates proliferation and induces apoptosis in ccRCC cells. SP1 was also found to regulate the expression of FBXL6.

## Introduction

Renal cell carcinoma (RCC) is a highly malignant tumor of the urinary system that is not susceptible to radiotherapy and chemotherapy [1]. Approximately 75–80% of the pathological types of RCCs are clear cell renal cell carcinoma (ccRCC) [2]. In recent years, with the improvement of modern medical standards and public health awareness, the detection rate of renal cancer has increased annually. Radical resection is the main treatment for renal cancer, and the postoperative cure rate is high. However, it is estimated that about 40% of patients will relapse after surgery [3,4]. In addition, once distant metastasis occurs in RCC, the long-term survival rate of patients is significantly reduced [5]. Tyrosine kinase inhibitors, mammalian target of rapamycin (mTOR) inhibitors, and immune checkpoint blockade have all been shown to be promising strategies in the treatment of RCC [6–8]. However, little is known about the best therapeutic approach to combat RCC and

therapeutic resistance in RCC. Therefore, there is an urgent need for a meticulous study of the occurrence and development of RCC to identify valuable prognostic markers that can be used for individualized clinical treatment.

The SCF complex is the most distinctive CRL1 member of the largest E3 ubiquitin ligase family [9,10], cullin-RING E3 ligase (CRL), also known as the SKP1-cullin 1-F-box protein (SCF) E3 ligase complex [11, 12]. Unlike other typical E3 ubiquitin ligases, scaffolds function primarily by relying on the F-box protein to target specific substrates and perform ubiquitination [11]. At present, there are an increasing number of studies on F-box family genes in tumors, and we screened nearly 70 F-box family genes using a series of bioinformatics methods. Furthermore, by constructing a risk prognosis model and nomogram, differentially expressed genes closely related to the overall survival (OS) of patients with ccRCC were identified, and FBXL6 was finally identified as the molecule of interest. We found that the research on FBXL6 in tumors

\* Corresponding author at: The First Affiliated Hospital of Harbin Medical University, No.23, Post Street, Nangang District, Harbin, 150001, China.

E-mail address: [doctorcheng77@163.com](mailto:doctorcheng77@163.com) (C. Zhang).

is limited. For example, in hepatic cancer, accumulation of FBXL6 promotes the stabilization and activation of c-Myc by preventing the degradation of HSP90AA1, wherein activated c-Myc binds directly to the promoter region of FBXL6 to induce mRNA expression [13]. In recent studies, FBXL6 was reported to be highly expressed and associated with poor prognosis in colorectal cancer, and mechanically, FBXL6 targets phosphorylated P53 (S315) to mediate its polyubiquitination and proteasome degradation, thereby inhibiting P53 signaling [14]. However, there are currently no studies on FBXL6 in RCC. The predictive prognosis potential of FBXL6 in patients with ccRCC and its function in renal cancer are unclear and need to be further elucidated.

SP1 was one of the first transcription factors discovered and is an important member of the Sp/Krüppel-like factors (Sp/KLF) family [15]. It is a DNA-binding protein that is highly expressed in most tumors and has a malignant phenotype; its abnormal activation can be involved in the pathogenesis of many tumors [16–18]. At present, the mechanism of SP1 in ccRCC is not clear, and previous studies have reported that SP1 knockdown significantly inhibits cell proliferation and induces cell cycle blocking in the G1 phase [19]. Significant elevation of SMYD3 expression in RCC tumors has been reported, and SP1 works with SMYD3 to promote EGFR expression and amplify its downstream signaling activity [20]. In another report, it was also demonstrated that SP1 induces upregulation of lncRNA SNHG14 as a competitive RNA, thereby promoting the migration and invasion of ccRCC by modulating N-WASP [21]. The above results show that high expression of SP1 plays an important role in the occurrence and development of ccRCC. Therefore, we hypothesized that SP1 could also be implicated in the development and progression of ccRCC by regulating the transcription of FBXL6.

Based on these previous studies, this study was designed to investigate the function of FBXL6 in ccRCC, which may provide new insights for exploring targeted therapies based on F-box proteins and substrates. In addition, combined with the gene signature of the F-box family, we also constructed a risk prognosis model and nomogram to quantify risk and benefit assessment.

## Materials and methods

### Data acquisition

We collected the F-box family gene list from the GeneCards database (<https://www.genecards.org/>) based on previous studies [22,23] (Supplementary Table 1). We also downloaded transcriptome data consisting of 72 normal renal samples and 539 ccRCC samples from The Cancer Genome Atlas database (TCGA, <https://portal.gdc.cancer.gov/>), and obtained the corresponding clinical information of all patients with ccRCC. In addition, GSE40435 [24] as a dataset from the Gene Expression Omnibus database (GEO, <https://www.ncbi.nlm.nih.gov/geo/>), contains gene expression profiling data for 101 pairs of ccRCC and adjacent tissues.

### Identification of differentially expressed F-box family genes in patients with ccRCC

We used the “edgeR” package to perform differential analysis of 72 normal kidney samples and 539 ccRCC samples to identify differentially expressed F-box family genes, with the screening criteria set to  $|\log_2FC| > 1.0$  and false discovery rate (FDR)  $< 0.05$ . The expression data were normalized using the default trimmed mean of M-values (TMM) method, and the expression of the same gene was averaged, while genes with a count value of less than 1 were removed. Volcano plots and heatmaps drawn by “ggplot2” and “pheatmap” packages were used for data visualization. The “corrplot” package was used to calculate the correlation coefficients among differential genes.

### Construction and validation of prognostic risk model

The “caret” package randomly divided the ccRCC dataset from TCGA into the training set and testing set. Univariate Cox regression analysis was performed using the Kaplan-Meier “survival” package on the differentially expressed F-box genes in the training set to screen for genes associated with OS ( $p < 0.05$ ), and a prognostic risk model was further constructed using multivariate Cox regression analysis. The risk score of each patient was calculated using the following equation:

$$\text{Risk score} = \sum_{i=1}^n (\text{coef}_i \times \text{Exp}_i)$$

**Coef** represents the regression coefficient of the F-box genes in the model, while **Exp** is the expression value of the gene. Patients in the training set were divided into high- and low-risk groups based on the median risk scores, and the differences in overall survival between the two groups were compared using the log-rank test. Time-dependent receiver operating characteristic (ROC) curves [25] drawn using the “timeROC” package were used to evaluate the predictive performance of the model. Simultaneously, we calculated the risk scores of patients in the testing set and the entire set separately, according to the same formula and obtained similar conclusions.

### Independent prognostic analysis and construction of nomogram

To identify whether the risk model we constructed was independent of prognostic factors for other clinical features, such as age, sex, pathological grade, and pathological stage, we performed univariate and multivariate Cox regression analyses. The analyses were performed using the coxph function to assess the relationship between the overall survival of patients with ccRCC and the risk score, along with other independent variables. Based on risk score and clinical parameters, we also constructed a nomogram to predict 1-, 3- and 5-year OS for patients with ccRCC by the “rms” package. Calibration curves and the C-index were used to assess the reliability of the nomogram.

### Cell culture and small interfering RNA (siRNA) transfection

Human RCC cell lines (786-O, OS-RC-2, and ACHN) and human renal tubular epithelial cells (HK-2) were all purchased from the Cell Resources Center, Shanghai Academy of Life Sciences, and Chinese Academy of Sciences. A498 cells were purchased from ATCC. All cell lines were authenticated by STR detection and cultured in the recommended medium supplemented with 10% heat-inactivated fetal bovine serum (Biological Industries, Israel) at 37°C with 5% CO<sub>2</sub>. Small interfering RNA (siRNA) was transfected into the cells according to the manufacturer’s instructions of jetPRIME (Polyplus, NY, USA). The specific siRNA sequences used to knock down FBXL6 and SP1 expression are listed in Supplementary Table 2.

### RNA isolation and quantitative RT-PCR

Total RNA was extracted from ccRCC cell lines using the RNA Quick Purification kit (Yishan, Shanghai, China) and reverse transcribed into cDNA using the PrimeScript RT Reagent Kit (TaKaRa, Japan) according to the manufacturer’s instructions. Gene expression levels were measured by reverse transcription-quantitative polymerase chain reaction (RT-qPCR) using TB Green Premix Ex Taq (TaKaRa, Japan). The  $2^{-\Delta\Delta CT}$  method [26] was used to analyze the data. PCR primers were synthesized using Tsingke (Beijing, China) and are listed in Supplementary Table 3.

### Western blot analysis and antibodies

The Cells were lysed using RIPA lysis buffer (Beyotime, Shanghai,

China). The quantified proteins were separated by SDS-PAGE and transferred to polyvinylidene fluoride (PVDF) membranes. The membranes were blocked with 5% BSA for 2 h at room temperature and incubated with the corresponding antibodies. The following primary antibodies were used as indicated: anti-FBXL6 (1:1000 dilution, HPA008867, Sigma; RRID:AB\_2668161), anti-SP1 (1:2000 dilution, 21962-1-AP, Proteintech; RRID:AB\_10898171), anti-PCNA (1:2000 dilution, 10205-2-AP, Proteintech; RRID:AB\_2160330), anti-Bcl2 (1:2000 dilution, 12789-1-AP, Proteintech; RRID:AB\_2227948), anti-Bax (1:5000 dilution, 50599-2-Ig, Proteintech; RRID:AB\_2061561), anti-c-Myc (1:1000 dilution, 5605, Cell Signaling Technology; RRID:AB\_2798629), and anti- $\beta$ -actin (1:5000 dilution, 66009-1-Ig, Proteintech; RRID:AB\_2687938). The secondary antibodies used were horseradish peroxidase-conjugated goat anti-mouse IgG (H+L) (1:5000 dilution, W4021, Promega; RRID:AB\_430834) and anti-rabbit IgG (H+L) (1:5000 dilution, W4011, Promega; RRID:AB\_430833). Enhanced chemiluminescence (ECL) kit was used for imaging with a chemiluminescence imaging system.

#### CCK-8 cell proliferation assay

The CCK-8 reagent (Beyotime, Shanghai, China) was added to the cell culture medium at a ratio of 1:10 and mixed. After incubation at 37°C for 2 h, absorbance was measured at 450 nm to assess cell viability.

#### EdU assay

The cells were inoculated on coverslips in 12-well plates at the appropriate cell numbers, and the following day, the EdU working solution was added to the cells for 2 h. The cells were then fixed and stained as per the manufacturer's instructions (Beyotime, Shanghai, China) and finally photographed using a fluorescent microscope.

#### Cell cycle and apoptosis assays

Cell cycle analysis was performed after transfection with siRNA. According to the Cell Cycle and Apoptosis Analysis Kit (Beyotime, Shanghai, China), cells were collected, fixed in 70% ethanol for 24 h, stained with propidium iodide (PI), and then cell cycle assays were performed using CytoFLEX S (Beckman, USA). Similarly, for apoptosis assays, cells were processed using the FITC Annexin V Apoptosis Detection Kit I (Becton Dickinson, USA) and then analyzed by flow cytometry. Finally, the results were analyzed using the FlowJo software.

#### Chromatin immunoprecipitation (ChIP)-qPCR

A ChIP Assay Kit (Beyotime, Shanghai, China) was used for the ChIP assay. Briefly, exponentially growing cells ( $1 \times 10^7$  cells) were cross-linked in 1% formaldehyde for 10 min. The total lysates were sonicated and subjected to immunoprecipitation using specific antibodies. Anti-SP1 (1:200 dilution, 21962-1-AP, Proteintech; RRID:AB\_10898171) and rabbit IgG were used as controls. The chromatin was then eluted with elution buffer, treated with proteinase K, and decross-linked. The enrichment level of the FBXL6 promoter was examined by qPCR. The primer sequences [14] of FBXL6 were as follows: #1, forward primer: 5'-CCTTTCTGCTGTGGAACACGTG-3'; reverse primer: 5'-GGCGTTGCCCTGGAGCAGGCAC-3'. #2, forward primer: 5'-GGGGCCACATGGTCCACAGAG-3'; reverse primer: 5'-CTCCCTTGGGCATCATGACCCT-3'.

#### Xenograft assay

Approximately  $5 \times 10^6$  ACHN cells (shCtrl and shFBXL6#1) in 100  $\mu$ l PBS per mouse were implanted subcutaneously into the flanks of male BALB/c nude mice. Tumor growth and volume were monitored regularly for up to 30 days. The mice were sacrificed and the tumors were

dissected and weighed. Animal experiments were performed in accordance with the National Institutes of Health Guide for the Care and Use of Laboratory Animals and were approved by the Animal Care and Use Committee of the First Affiliated Hospital of Harbin Medical University. The shRNA lentiviral vector was constructed by Hanbio (Shanghai, China) and the sequences are listed in Supplementary Table 4.

#### Statistical analysis

The results are shown as mean  $\pm$  standard deviation (mean  $\pm$  SD) of at least three biological replicates. Student's *t*-test was used for comparisons between two groups, and comparisons among multiple groups were analyzed by one-way ANOVA. Statistical analysis was performed using GraphPad Prism 9.0 and R software (version R-4.1.0). Statistical significance is shown as \*  $p < 0.05$ , \*\*  $p < 0.01$ , and \*\*\*  $p < 0.001$ .

## Results

### Screening for differentially expressed F-box family genes in ccRCC

Post-translational modifications, including ubiquitination, have been reported to play an important role in ccRCC. An important part of the SCF complex, the F-box family, is involved in a variety of cell biology processes [27]. In this study, we constructed a prognostic risk model for ccRCC based on F-box family genes. Firstly, we downloaded transcriptome data from 72 normal kidney samples and 539 ccRCC samples from TCGA, and collected 69 F-box family genes from previous studies. We identified 12 differentially expressed F-box family genes in ccRCC using the "edgeR" package (screening criteria  $|\log_2FC| > 1.0$ , FDR  $< 0.05$ ). The  $\log_2FC$  values of these differentially expressed genes and their *p*-values are listed in Supplementary Table 5. Compared with normal kidney samples, there were 10 upregulated genes (FBXO39, FBXO41, FBXL8, FBXO43, FBXL16, FBXO17, FBXL21, FBXL6, FBXO6, and FBXO1) and 2 downregulated genes (FBXO20 and FBXO2) in ccRCC samples (Fig. 1A-B). In addition, these 12 genes correlated with each other (Fig. 1C).

### Construction and evaluation of prognostic risk model based on F-box family genes

We randomly divided 530 ccRCC sample transcriptome data from TCGA into a training set (371 cases) and a testing set (159 cases) using the "caret" R package. We first performed univariate Cox regression analysis of transcriptome data of differentially expressed F-box family genes in the training set and identified that 8 of the 12 genes (FBXO20, FBXO39, FBXO43, FBXO41, FBXL6, FBXO1, FBXO6, and FBXL16) were associated with the OS of patients with ccRCC ( $p < 0.05$ ) (Supplementary Table 6). Multivariate Cox regression analyses showed that 4 of the 8 genes (FBXO39, FBXL6, FBXO1, and FBXL16) were independent prognostic markers associated with the OS of patients with ccRCC. Finally, these genes were used to construct a risk model to assess the prognostic risk of ccRCC (Supplementary Table 7). The risk score for each patient was calculated according to the following formula: Risk score =  $(0.15666 \times \text{Exp FBXO39}) + (0.30211 \times \text{Exp FBXL6}) + (0.35929 \times \text{Exp FBXO1}) + (-0.11216 \times \text{Exp FBXL16})$ .

Based on the median prognosis risk score of 0.9336, we divided the 371 ccRCC samples from the training set into low- and high-risk groups. Kaplan-Meier survival curve analysis showed that the low-risk group had a longer survival time ( $p < 0.0001$ ) than that of the high-risk group (Fig. 1D). Fig. 1E shows the survival status of each patient in the training set, assessed by the risk score. As the risk score increased, the survival status worsened. To evaluate the predictive performance of this risk model, we performed a time-dependent ROC curve analysis, and the area under the ROC curve (AUC) of the model was 0.73, 0.702, and 0.716 at 1-year, 3-year, and 5-year, respectively (Fig. 1F), indicating that this risk model has good sensitivity and specificity for predicting the

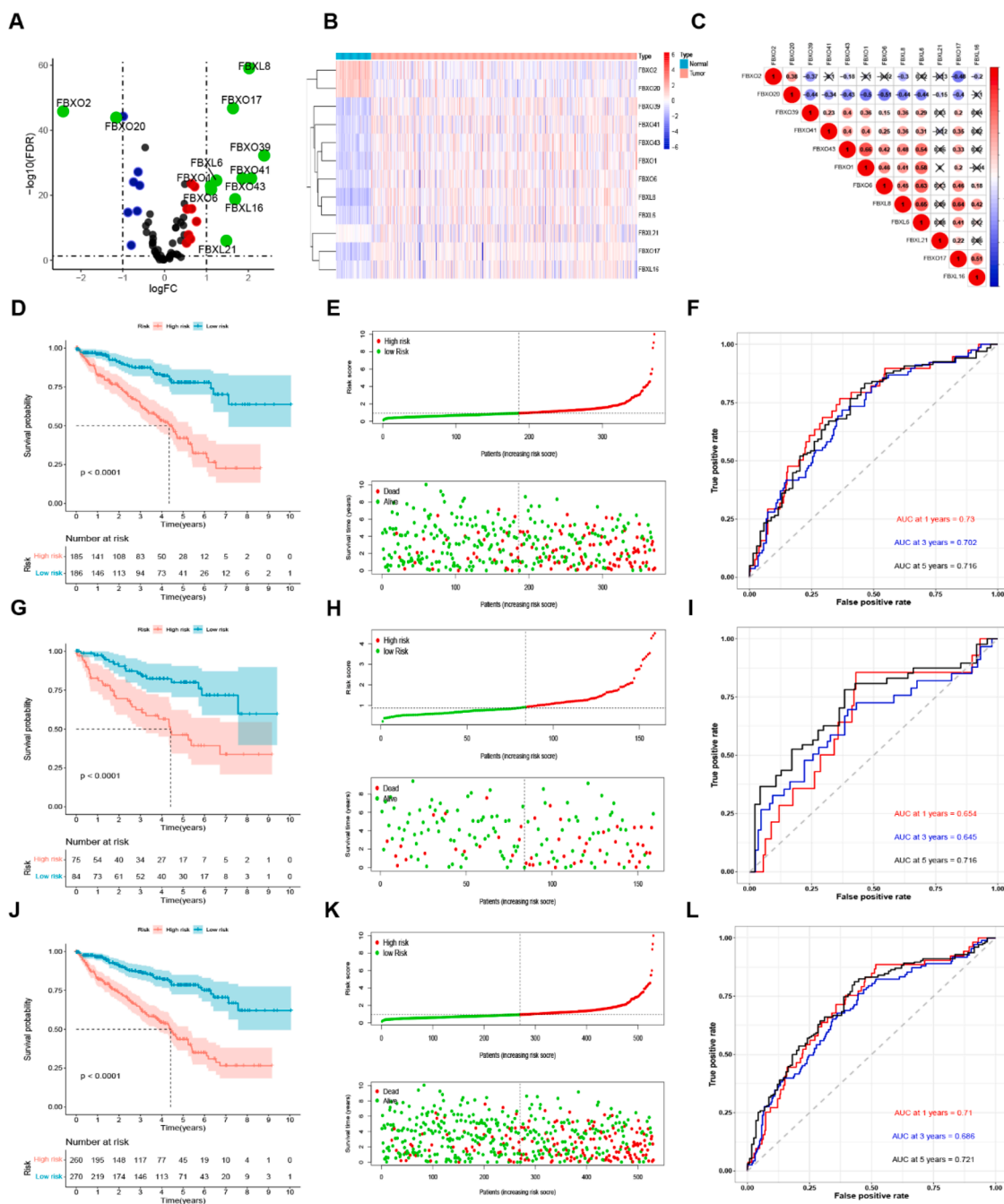


**Fig. 1.** Identification of differentially expressed F-box family genes and construction of prognostic model in TCGA. (A) The volcano plot showed the upregulated or downregulated F-box family genes in ccRCC. (B) The heatmap showed the expression of 12 differentially expressed F-box family genes in 539 ccRCC and 72 normal kidney samples. (C) Pearson correlation analysis of the 12 F-box family genes in ccRCC. (D) Kaplan-Meier survival curve showed the relationship between the high-risk group (185 cases) and the low-risk group (186 cases) and the overall survival in the training set ( $p < 0.05$ ). (E) The relationship between survival status and risk score of high- and low-risk groups in the training set. (F) Time-dependent ROC curve showed that the model predicts the survival rate of high- and low-risk groups at 1, 3, and 5 years in the training set. (G) and (J) The KM survival curve showed the relationship between the high- and low-risk groups in the testing and entire sets and overall survival ( $p < 0.05$ ). (H) and (K) The relationship between survival status and risk score for the high- and low-risk group in the testing and entire sets. (I) and (L) Time-dependent ROC curve showed that the model predicts the survival rate of the high- and low-risk groups at 1, 3, and 5 years in the testing and entire sets.

prognosis of patients with ccRCC. We also applied the same risk score formula to calculate the risk scores of patients in the testing and entire sets and further validated our model by classifying patients into high- and low-risk groups using 0.9336 as the cutoff value, obtaining the same conclusions as for the training set (Fig. 1G-L). These results demonstrate the reliability of the prognostic model.

*Assessment of independent prognostic markers and construction of Nomogram*

To determine whether the F-box family gene signature is an independent prognostic factor for patients with ccRCC, we performed univariate and multivariate Cox regression analyses on patients from TCGA. Univariate Cox regression analysis showed that six clinical characteristics (age, grade, stage, T, M, and N) and the risk score based on the F-box

gene signature model were significantly associated with OS ( $p < 0.05$ ), except for sex (Fig. 2A). Multivariate Cox regression analysis showed that only age, clinical stage, and risk score were independent prognostic factors associated with OS in patients with ccRCC ( $p < 0.05$ ) (Fig. 2B). In addition, to establish a method for quantitatively assessing the prognosis of patients with ccRCC, we constructed a nomogram based on the above independent prognostic factors (Fig. 2C). By drawing a vertical line on each prognostic factor axis and scoring axis and finally summarizing the total score, we can predict the incidence of OS in patients with ccRCC at 1, 3, and 5 years. At the same time, we calculated the C-Index, which is 0.776, to determine the reliability of the model. A calibration curve was constructed to evaluate the nomogram, and the results showed that the predicted results of the method were in good agreement with the actual results (Fig. 2D), confirming the reliability and accuracy of the nomogram. This may help clinical practitioners make clinical decisions about patients with ccRCC and provide valuable insights into individualized treatment.

Screening of the prognostic valuable gene FBXL6 and its relationship with clinical features

Firstly, we determined the relationship between the F-box family genes and OS using the Kaplan-Meier plotter (<http://kmplot.com/analysis/index.php?p=background>) online tool [28]. The survival curve showed that all four F-box family genes were significantly associated with OS in patients with ccRCC (Fig. 3A and Fig. S1A). However, all four genes were highly expressed in patients with ccRCC, and the survival curve of FBXL6 showed a poor prognosis for low expression, which was not in line with expectations. Secondly, we used the FPKM transcriptome data of ccRCC in TCGA to plot the diagnostic ROC curves, as shown in Fig. 3B and Fig. S1B, the AUC values of FBXO39, FBXL6, FBXO1 (also known as CCNF), and FBXL16 were 0.870, 0.866, 0.871 and 0.782, respectively. After reviewing the literature, we finally chose FBXL6 as the molecule of interest because there are no relevant studies reported in ccRCC.

To explore the relationship between FBXL6 and clinical features in

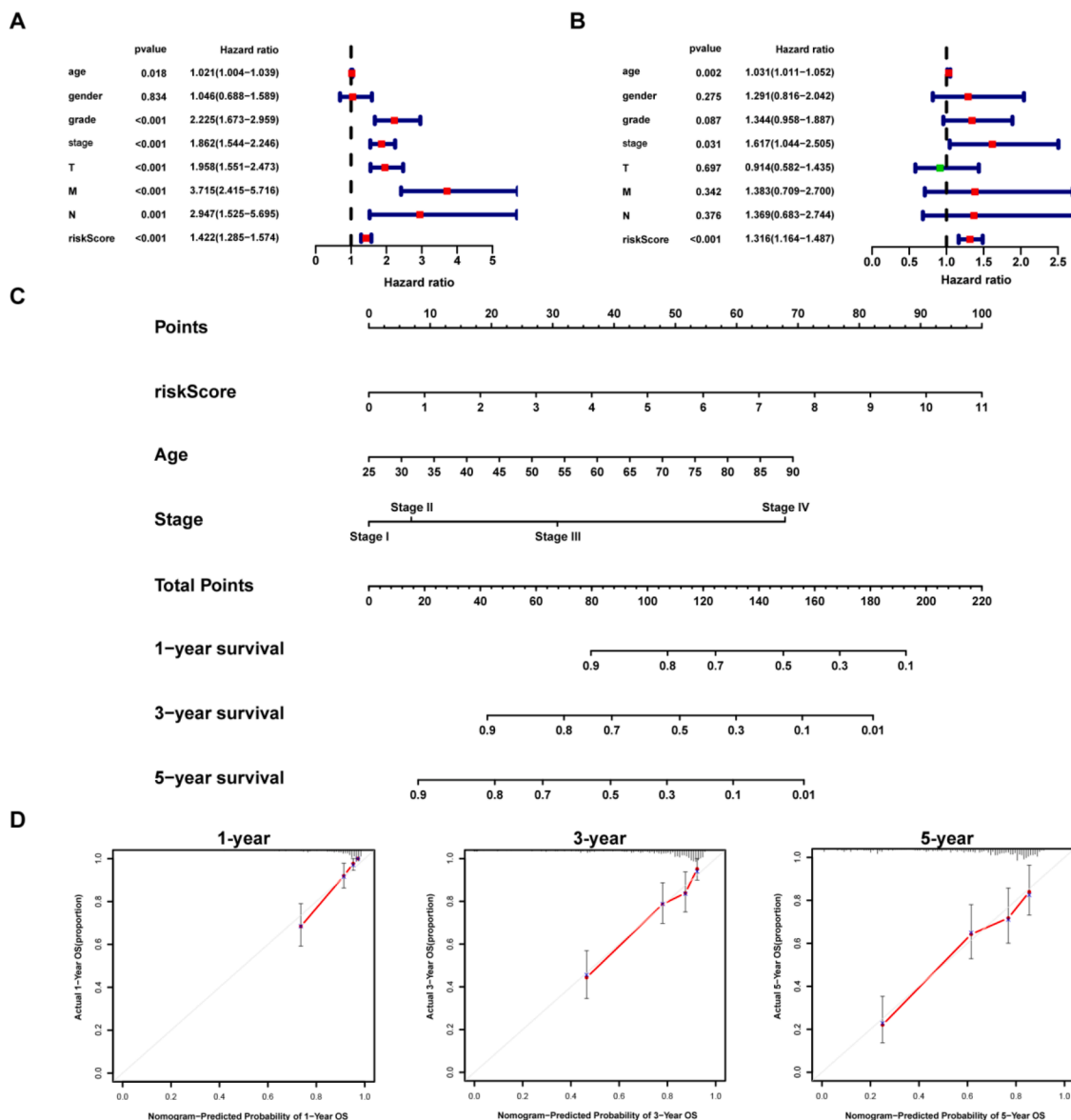
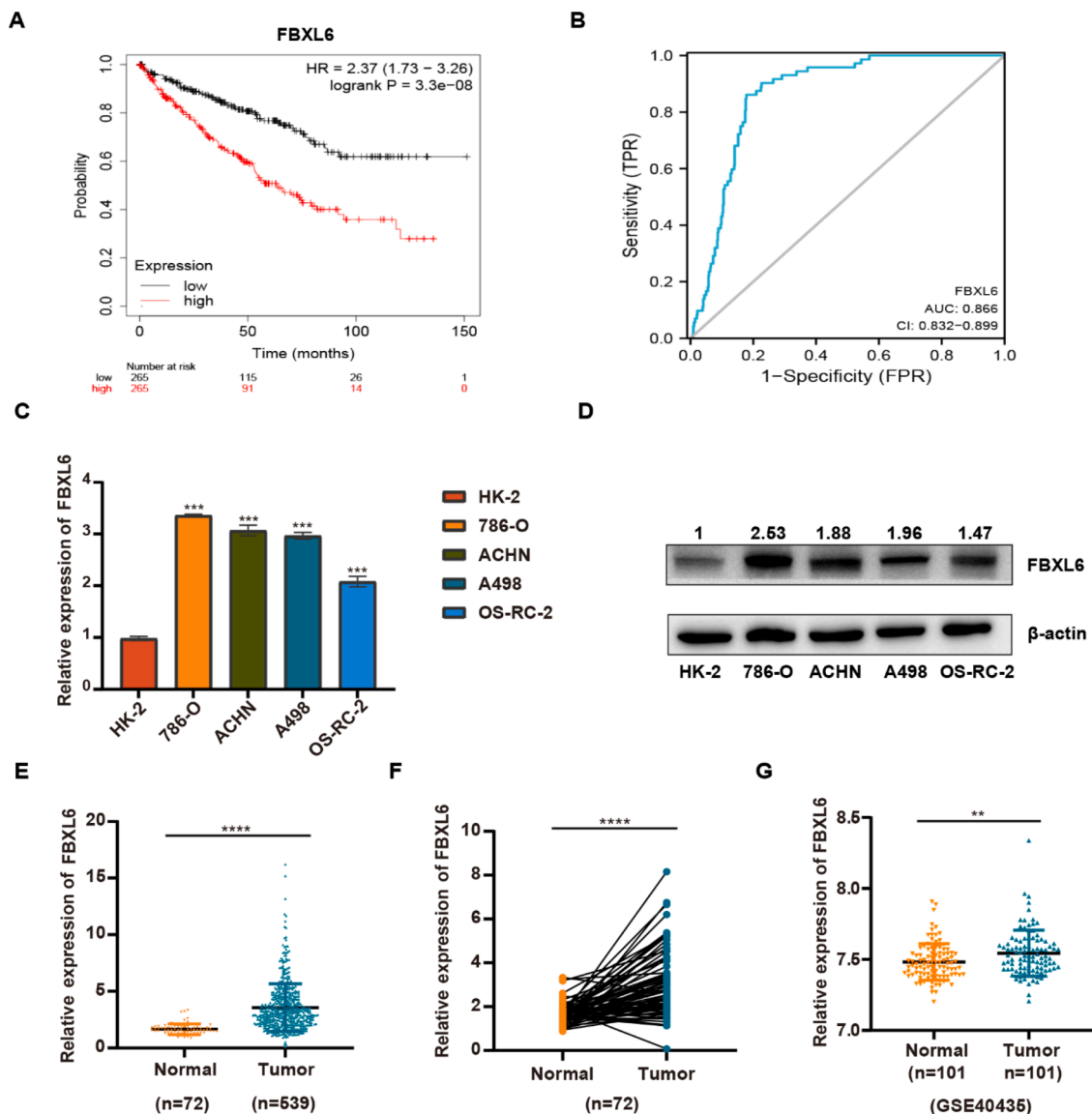


Fig. 2. Construction of a nomogram and assessment of the prognostic significance of different clinical characteristics in patients with ccRCC. (A-B) Univariate Cox and multivariate Cox regression analysis showed a statistical difference between clinical characteristics and risk score and overall survival ( $p < 0.05$ ). (C) Nomogram based on F-box family gene risk score and clinical-pathological parameters predicted survival rates in patients with ccRCC at 1, 3, and 5 years. (D) Calibration curves showed consistency between the prediction and the actual observed 1-year, 3-year, and 5-year survival rates.



**Fig. 3.** FBXL6 is highly expressed in ccRCC cell lines and tumors. (A) The Kaplan–Meier plotter online database was used to demonstrate the survival curve of FBXL6. (B) The diagnostic ROC curves of FBXL6 were plotted by R using ccRCC transcriptome data in TCGA. (C) mRNA expression levels of FBXL6 in normal tubular epithelial cells HK-2 and ccRCC cell lines 786-O, ACHN, A498, and OS-RC-2. (D) Protein expression levels of FBXL6 in the above cells. (E) Differences in mRNA expression levels of FBXL6 between 539 ccRCC samples and normal kidney samples in TCGA. (F) Differences in mRNA expression levels of FBXL6 between 72 paired ccRCC samples and adjacent tissues in TCGA. (G) Differences in mRNA expression levels of FBXL6 between 101 paired ccRCC samples and adjacent tissues in the GSE40435 dataset. For cellular experiments, three repetitions were performed. \*  $p < 0.05$ , \*\*  $p < 0.01$ , and \*\*\*  $p < 0.001$ .

patients with ccRCC, we confirmed using chi-square test that clinical features, including clinical stage, T stage, M stage, Fuhrman grade, and survival status, were significantly different between the high- and low-expression groups of patients with ccRCC (Table 1). In addition, we incorporated variables such as age, sex, clinical stage, TNM stage, Fuhrman grade, and FBXL6 expression level into univariate and multivariate Cox regression analyses and found that the mRNA expression level of FBXL6 and the age of patients were independent prognostic factors for patients with ccRCC (Table 2). To date, data have shown that FBXL6 is an independent prognostic factor in ccRCC, and its high expression indicates a poor prognosis.

#### FBXL6 expression is upregulated in ccRCC cell lines and tumors

To further confirm the expression of FBXL6 in ccRCC, we detected the mRNA and protein level expression of FBXL6 in five cell lines (HK-2, 786-O, ACHN, A498, and OS-RC-2) through RT-qPCR and western blot

assays. The results showed that the mRNA and protein levels of FBXL6 in ccRCC cell lines were upregulated as compared to that in HK-2 cells. This difference was statistically significant ( $p < 0.05$ ) (Fig. 3C–D).

The mRNA expression level of FBXL6 was significantly higher ( $p < 0.0001$ ) in 539 ccRCC samples than that in 72 normal kidney samples from TCGA (Fig. 3E). The same conclusion was drawn for 72 paired ccRCCs and adjacent tissues ( $p < 0.0001$ ) (Fig. 3F). This conclusion was also confirmed in dataset GSE40435, where the mRNA expression levels of FBXL6 in 101 pairs of ccRCC and adjacent tissues are shown in Fig. 3G ( $p < 0.005$ ). The above results showed that FBXL6 was highly expressed in patients with ccRCC from a public database and ccRCC cell lines, and also had good diagnostic guidance, with the sensitivity and specificity of the diagnostic ROC curve being 82.2 and 86.1%, respectively.

#### Depletion of FBXL6 inhibits cell proliferation and induces apoptosis

To verify the role of FBXL6 in the development of ccRCC, we

**Table 1**  
Relationship between FBXL6 expression levels and clinical features in 530 ccRCC patients.

Characteristic	Variable	High expression of FBXL6	Low expression of FBXL6	$\chi^2$	<i>p</i>
All patients		265	265		
Gender	Female	93 (17.5%)	93 (17.5%)	0	1
	Male	172 (32.5%)	172 (32.5%)		
Age	>60	139 (26.2%)	127 (24%)	0.91	0.339
	≤60	126 (23.8%)	138 (26%)		
Stage	Stage I	104 (19.7%)	161 (30.6%)	35.59	< 0.001
	Stage II	24 (4.6%)	33 (6.3%)		
	Stage III	77 (14.6%)	46 (8.7%)		
	Stage IV	58 (11%)	24 (4.6%)		
T stage	T1	108 (20.4%)	163 (30.8%)	28.17	< 0.001
	T2	34 (6.4%)	35 (6.6%)		
	T3	117 (22.1%)	62 (11.7%)		
	T4	6 (1.1%)	5 (0.9%)		
N stage	N0	116 (45.5%)	123 (48.2%)	0.68	0.41
	N1	10 (3.9%)	6 (2.4%)		
M stage	M0	184 (36.9%)	236 (47.4%)	17.74	< 0.001
	M1	55 (11%)	23 (4.6%)		
Fuhrman grade	G1	5 (1%)	9 (1.7%)	31.54	< 0.001
	G2	89 (17%)	138 (26.4%)		
	G3	112 (21.5%)	94 (18%)		
	G4	56 (10.7%)	19 (3.6%)		
Vital status	dead	118 (22.3%)	48 (9.1%)	41.76	< 0.001
	alive	147 (27.7%)	217 (40.9%)		

Note: The bold *p* values reflect a significant difference.

explored the effect of FBXL6 expression on the tumor biological function of ccRCC through a series of experiments. First, we validated the efficiency of knocking down FBXL6, including the mRNA and protein levels, in 786-O and ACHN cells (Fig. 4A). The effect of knockdown FBXL6 on the proliferative capacity of ccRCC cells was examined using the CCK-8 assay (Fig. 4B). The results showed that in both 786-O and ACHN cells, the proliferative capacity of the cells was significantly inhibited after knockdown of FBXL6 compared to the control group. This conclusion was further confirmed by the EdU assay, as shown in Fig. 4C, after knocking down FBXL6, the DNA replication activity within the two kinds of cells was significantly inhibited. At the same time, we also detected the expression of PCNA, a proliferation-related marker gene, through a western blot assay, and found that the expression of PCNA was

**Table 2**  
Clinical pathologic characteristics of 246 ccRCC patients and association between FBXL6 expression and these variables.

Parameter	Univariate analysis			Multivariate analysis		
	HR	95%CI	<i>p</i>	HR	95%CI	<i>p</i>
Age	1.023	1.005-1.041	<b>0.012</b>	1.031	1.011-1.051	<b>0.002</b>
Gender	1.013	0.666-1.541	0.951	1.414	0.887-2.255	0.146
Grade	2.242	1.682-2.988	<b>3.61E-08</b>	1.281	0.91-1.803	0.156
Stage	1.862	1.541-2.251	<b>1.26E-10</b>	1.161	0.672-2.004	0.593
T classification	1.943	1.538-2.456	<b>2.69E-08</b>	1.190	0.715-1.978	0.504
N classification	2.932	1.516-5.668	<b>0.001384</b>	1.227	0.574-2.621	0.598
M classification	4.073	2.634-6.3	<b>2.76E-10</b>	2.336	0.998-5.465	0.050
FBXL6	1.923	1.49-2.481	<b>5E-07</b>	1.567	1.161-2.114	<b>0.003</b>

Note: The bold *p* values reflect a significant difference.

significantly inhibited after knockdown of FBXL6.

In addition, we examined the cell cycle and apoptosis using flow cytometry to demonstrate the effect of FBXL6 knockdown on the cell cycle and apoptosis. In the two cell types, after inhibiting the expression of FBXL6, the cell cycle was blocked in the S phase, and the difference was statistically significant (*p* < 0.05) (Fig. 4D). Similarly, early and late cell apoptosis increased significantly after depletion of FBXL6 (Fig. 4E). This conclusion was also confirmed by western blotting, and we found that after knocking down FBXL6, the apoptosis inhibitor Bcl2 decreased significantly, while the apoptosis promoter Bax increased, and the difference was statistically significant (Fig. 4F). Finally, in order to explore the underlying mechanisms behind the influence of cell proliferation and apoptosis, based on similar studies in previous researches [13], we confirmed that depletion of FBXL6 decreases c-Myc protein levels (Fig. 4G). Therefore, we speculated that FBXL6 may regulate the progression of ccRCC by affecting the accumulation of c-Myc. However, we failed to demonstrate the underlying mechanism, which needs to be further investigated in future.

#### SP1 silencing suppresses transcription of FBXL6

The downstream mechanism of FBXL6 in other tumors has been reported, the upstream mechanism has not yet been studied. Therefore, we aimed to explore the transcriptional regulation mechanism of this gene. While screening for possible binding transcription factors using the UCSC (<http://genome.ucsc.edu/>) database, we found that there was a star transcription factor SP1 among the predicted transcription factors; therefore, we chose SP1 for validation. Firstly, we detected the mRNA and protein levels of SP1 and FBXL6 by RT-qPCR and western blot, and the results showed that after knocking down SP1, the mRNA and protein level expression of FBXL6 were significantly downregulated, and the difference in results was statistically significant (Fig. 5A). Finally, to confirm whether SP1 can directly bind to the FBXL6 promoter to induce its transcription, we confirmed the binding of SP1 with the FBXL6 promoter region using the ChIP-qPCR assay (Fig. 5B). This suggested that SP1 regulates the expression of FBXL6 at the transcriptional level.

#### FBXL6 downregulation inhibits ccRCC tumor growth in vivo

To further investigate the effect of FBXL6 on ccRCC tumor growth in vivo, we constructed a cell line ACHN that interferes with FBXL6 expression with stable lentiviral transfection (negative control group shCtrl and FBXL6 interference group shFBXL6#1, shFBXL6#2), whose knockdown efficiency was assessed by western blotting (Fig. 5C). The volume and weight of subcutaneous tumors in the two groups of mice are shown in Fig. 5D-F, and the subcutaneous tumor volume and average weight of the knockdown FBXL6 group were significantly lower than those in the control group. Furthermore, IHC staining showed that the expression of the proliferation marker Ki67 was significantly lower (Fig. 5G). The results showed that FBXL6 downregulation significantly inhibited ccRCC tumor growth in vivo.

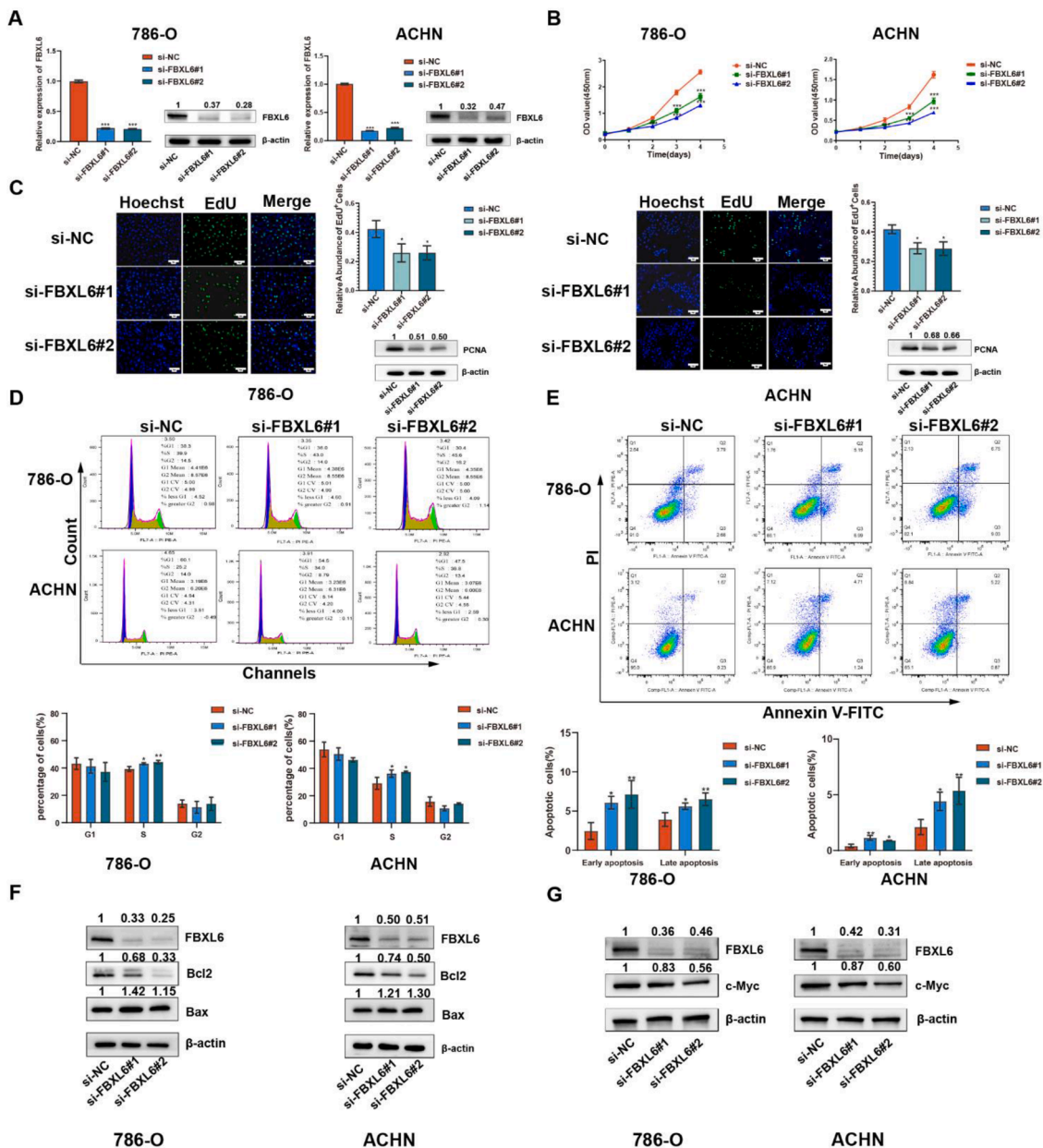


**Fig. 4.** FBXL6 knockdown inhibits cell proliferation and induces apoptosis. (A) Validation of knockdown FBXL6 efficiency in 786-O and ACHN cells. (B) CCK-8 assays showed the proliferative capacity of cells after knockdown FBXL6. (C) EdU assays and western blot confirmed that after the depletion of FBXL6 in ccRCC cells, both DNA replication and the expression of PCNA were inhibited. (D) Flow cytometry analysis showed the cell cycle of the knockdown FBXL6 group and control group in ccRCC cells. The distribution of the cell cycle was shown (left) and the histogram of the average percentage of G1, S, and G2 phases (right). (E) Flow cytometry showed that after knockdown FBXL6, the early and late apoptosis of both cells increased significantly. (F) Western blot analysis of Bcl2 and Bax after the depletion of FBXL6 in ccRCC cells. (G) FBXL6 depletion reduces c-Myc protein levels. For cellular experiments, the results were obtained from three independent experiments and are expressed as the mean  $\pm$ SD. \*  $p < 0.05$ , \*\*  $p < 0.01$ , and \*\*\*  $p < 0.001$ .

**Discussion**

As an important component of post-translational modifications, ubiquitination plays an important role in numerous biological processes such as cell cycle, apoptosis, and DNA damage repair, and their study in tumors is gaining increasing attention [29]. And an important enzyme that mediates ubiquitination modifications is an E3 ubiquitin ligase, which determines the specificity of substrate ubiquitination and degradation [30]. CRL1 is the most characteristic member of E3 ubiquitin ligases, also known as the SCF complex. The specificity of the SCF complex to perform its biological function depends mainly on its F-box protein, as it can target and recognize specific substrates for ubiquitination [10,31]. The current understanding demonstrates that F-box

proteins play an essential role in tumorigenesis mainly by regulating substrate turnover, which could be both in an E3 ligase activity-dependent or activity-independent manner [32–34]. In particular, multiple F-box proteins are attractive therapeutic targets for cancer treatment because of the correlation between their deregulation and tumorigenesis. However, most F-box proteins remain functionally enigmatic or "orphans" with no defined substrates, and our lack of understanding of these orphans is a major obstacle to the development of novel F-box protein-targeted therapies. Undoubtedly, as the substrates and functions of these orphan F-box proteins have been elucidated, additional drug targets will become apparent. Finally, with the development of personalized medicine, there is great promise for situational or context-dependent applications of SCF complex inhibitors. The

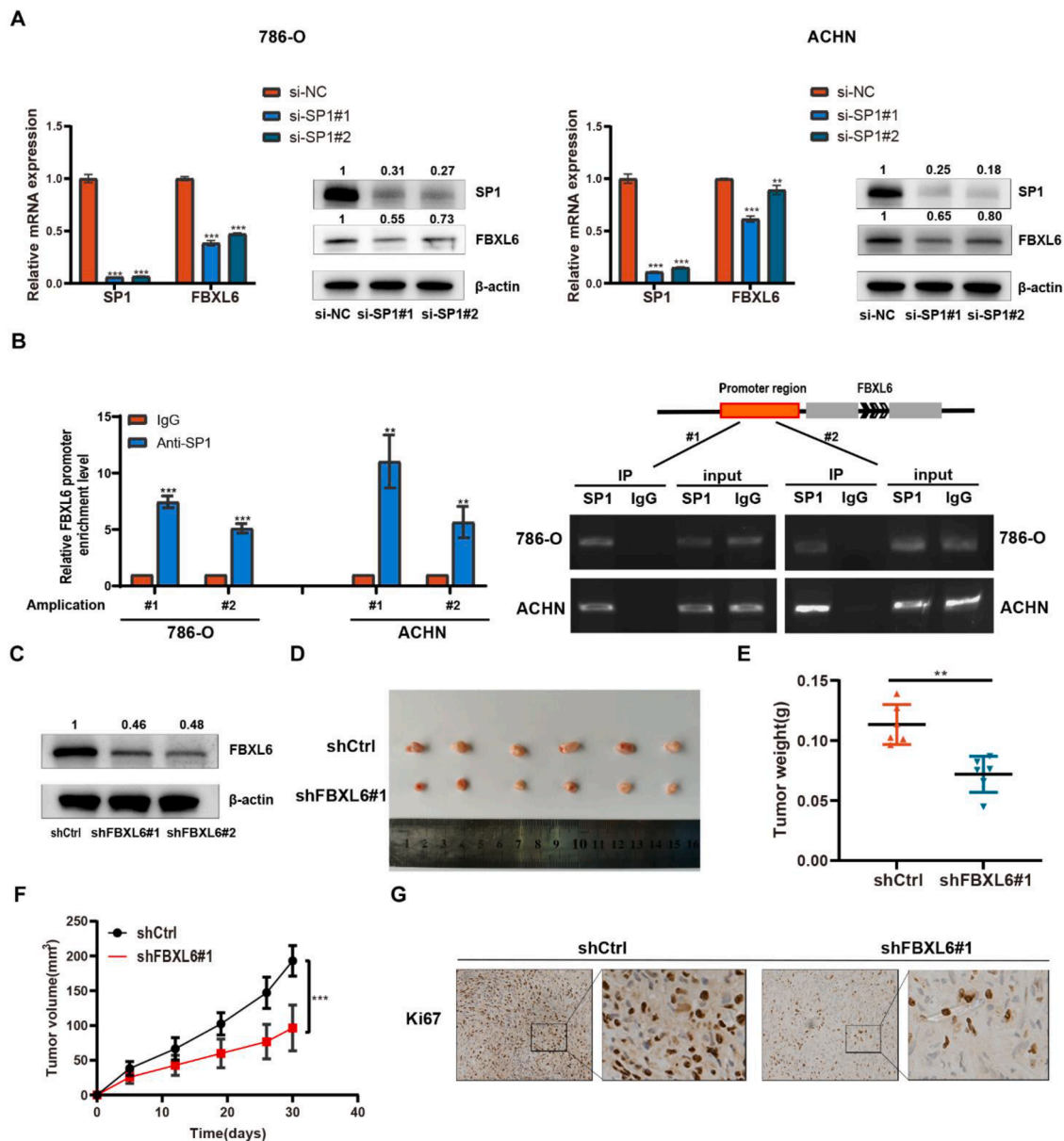


**Fig. 5.** Depletion of SP1 inhibits transcription of FBXL6. (A) Depletion of SP1 in 786-O and ACHN cells inhibited the mRNA and protein expression of FBXL6. (B) FBXL6 promoter sequence enriched by anti-SP1 in the ChIP-qPCR assay. #1 and #2 represent two different primers of FBXL6 from previous studies. (C) The efficiency of knockdown FBXL6 was confirmed by western blotting. (D) Subcutaneous xenograft tumor images of nude mice derived from shCtrl and shFBXL6#1 treated ACHN cells. (E) Differences in subcutaneous tumor weights between the two groups. (F) Differences in subcutaneous tumor volumes from two different groups. (G) Immunohistochemistry (IHC) staining of the proliferation marker Ki67 between the two groups. Tumor volumes and weights were measured every 3 days. For cellular experiments, three repetitions were performed; for animal experiments, n = 6 in each group. All values are mean ± SD. Student t-tests were used. \* p < 0.05, \*\* p < 0.01, and \*\*\* p < 0.001. SD, the standard deviation of the mean.

reports on F-box proteins in tumors is increasing annually; however, there are few studies on RCC. For example, FBXO22 significantly limited RCC cell migration and invasion, thereby reversing epithelial-mesenchymal transition (EMT), increasing the activity of tissue inhibitor of matrix metalloproteinase-1, and inhibiting metalloproteinase-9 (MMP-9) expression and activity in vitro [35]. Another study reported that upregulation of FBXW7 inhibited RCC metastasis and EMT, by regulating the expression of MMP-2, MMP-9, and MMP-13 [36]. In a study targeting cell cycle progression, MTORC2 signaling in RCC was reported to promote the G1-S phase transition of the cell cycle by increasing the protein expression of SKP2 and promoting the reduction of nuclear p27 protein levels [37]. Thus, exploration of F-box family genes could provide new perspectives on the pathogenesis of ccRCC and the discovery of potential drug targets.

With the progress of tumor multi-omics research, a large number of genes associated with tumor prognosis have been identified through bioinformatics analysis. In this study, we explored the differential F-box genes between 539 ccRCC and 72 normal kidney samples using the KIRC dataset from TCGA to identify potential biomarkers. We first analyzed the differential gene expression between ccRCC and normal kidney samples using the “edgeR” package in R, and 12 differentially expressed F-box genes were screened. Subsequently, the screening conditions were set and a risk prognostic model based on the F-box gene signature was constructed by univariate and multivariate Cox regression analyses, and four key prognostic-related genes (FBXO39, FBXL6, FBXO1, and FBXL16) were identified. The time-dependent ROC curves of this model in the training set showed AUC values of 0.73, 0.702, and 0.716 at 1, 3, and 5 years, respectively. To verify the predictive effect of the model, the

AUC values were found to be 0.654, 0.645, 0.716, and 0.71, 0.686, and 0.721 after validation of the testing and entire set, respectively. These results indicate the good predictive efficacy of the model. The risk score of each patient was calculated according to the established prognostic model formula, and then the patients were divided into high- and low-risk groups according to a median risk score of 0.9336, which showed that the prognosis of patients in the high-risk group was worse. At the same time, a nomogram was constructed based on the risk score combined with other independent prognostic factors, so that clinicians could make a comprehensive assessment of the patient's risk based on the model and actively adjust the patient's treatment plan, leading to individualized treatment.

To further explore the function of the above four key prognostic genes, we reviewed the literature and found that FBXO39 was highly expressed in invasive ductal carcinoma compared with normal human breast tissue [38]. It was also suggested that breast cancer patients with high FBXO39 expression have a poor prognosis [39]. Knockdown of FBXO39 expression in human osteosarcoma cells significantly inhibits cell proliferation and promotes apoptosis, suggesting a role for this gene in the development of osteosarcoma. The mRNA and protein levels of FBXO1 (also known as CCNF or Cyclin F) fluctuate during the cell cycle, suggesting that Cyclin F is dependent on cell cycle activity [40]. Cyclin F accumulated gradually during the G1/S transition phase of the cell cycle, reaching a peak in the G2 phase, while protein levels were downregulated because they were degraded by the ubiquitin-proteasome during mitosis and the G1 phase [41]. In addition, cyclin F is involved in ubiquitination and degradation of several cell cycle proteins [42]. These results suggest that dynamic regulation of cyclin F and substrate data highlights its importance in cell cycle regulation. For example, cyclin F promotes proliferation through the SCF-dependent degradation of the RB family protein P130/RBL2 [43].

It has also been shown that in lung cancer cell lines FBXL16 promoted cell growth, migration, and clone formation, mechanistically by antagonizing the activity of another F-box protein, FBW7, and increasing the stability of c-Myc [44]. However, in triple-negative breast cancer, FBXL16 is a tumor suppressor, and FBXL16 binds directly to HIF1 $\alpha$ , mediating the ubiquitination and degradation of HIF1 $\alpha$ , leading to HIF1 $\alpha$ -mediated EMT and blocked angiogenesis in breast cancer [45]. Additionally, studies on FBXL6 in tumors are limited, with only two articles on hepatocellular carcinoma and colon cancer and no reports on RCC. In hepatocellular carcinoma, the accumulation of FBXL6 promotes the stabilization and activation of c-Myc by preventing the degradation of HSP90AA1, where activated c-Myc binds directly to the promoter region of FBXL6 to induce its mRNA expression [13]. In a recent study, it was also found that high expression of FBXL6 in colorectal cancer was associated with poor prognosis, while FBXL6 targeted phosphorylated P53 (S315) to mediate its polyubiquitination and proteasomal degradation, thereby inhibiting P53 signaling [14].

To screen out the target genes, we performed a survival analysis using the Kaplan-Meier Plotter, an online database, and found that among them, the survival curve for FBXL16 showed a poor prognosis for low expression, which was unexpected. Diagnostic ROC curves were performed for the above genes to screen for prognostic indicators with good diagnostic potential (FBXO39 and FBXL6). Next, the expression of FBXO39 and FBXL6 was confirmed by qPCR experiments to be higher in ccRCC cell lines than in normal renal cell lines, but the Cq value of FBXO39 was too high, suggesting a lower expression level of this gene. Therefore, we finally selected FBXL6 as the study subject. Our study showed that the mRNA and protein levels of FBXL6 were higher in ccRCC cell lines than in renal tubular epithelial cells HK-2. In 786-O and ACHN cell lines, cell proliferation was inhibited, and apoptosis was induced upon depletion of FBXL6. This biological process may be achieved by altering the accumulation of c-Myc. Similarly, subcutaneous tumor growth was significantly inhibited in nude mice after the downregulation of FBXL6. In addition, we explored the upstream mechanism of FBXL6, and the results showed that the transcription factor SP1

regulated the expression of FBXL6 at the transcriptional level. Mechanistically, we confirmed that SP1 binds to the promoter region of FBXL6 using a ChIP-qPCR assay. Notably, when 786-O cells were treated with CHX (10  $\mu$ g/mL), FBXL6 depletion extended the half-life of endogenous p53 in 786-O cells (Fig. S1C), similar to previous studies [14]. Finally, we also showed the effect of FBXL6 depletion on MYC and p53 downstream genes (Fig. S1D). However, there are still some limitations of our study. For example, the mechanism by which FBXL6 affects the level of c-Myc protein remains unclear. As an E3 ubiquitin ligase, it affects the degradation of target proteins directly or indirectly through ubiquitination. This requires further investigation in future. In addition, the present study lacks validation with clinical samples. Overall, these findings suggest a potential oncogenic role for FBXL6 in ccRCC, supporting the importance of our prognosis model.

## Conclusions

In conclusion, we screened differentially expressed F-box family genes in ccRCC using bioinformatics methods and constructed a risk prognostic model based on the F-box gene signature after univariate and multivariate Cox regression analyses. Combined with the clinicopathological features, we drew a nomogram to quantify and comprehensively assess the prognostic risk of patients with ccRCC, to assist clinicians in decision-making, and for individualized treatment of patients. We confirmed that the F-box family gene FBXL6 can be used as a diagnostic and prognostic marker for patients with ccRCC and also explored the molecular function and oncogenesis of FBXL6.

## Availability of data and materials

The datasets used and/or analyzed during the current study are available from the corresponding authors on reasonable request.

## Funding

This work was supported by the National Natural Science Foundation of China (Grant Numbers 81872084) and Natural Science Foundation of Zhejiang Province (Grant Numbers LZ22H160008).

## CRediT authorship contribution statement

**Yongchun Yu:** Conceptualization, Methodology, Validation, Writing – original draft, Writing – review & editing. **Wenhao Yao:** Data curation, Validation, Writing – original draft, Writing – review & editing. **Tengda Wang:** Validation, Writing – original draft. **Wei Xue:** Validation, Formal analysis. **Yuyang Meng:** Formal analysis, Visualization. **Licheng Cai:** Formal analysis, Writing – review & editing. **Wengang Jian:** Formal analysis, Writing – review & editing. **Yipeng Yu:** Writing – review & editing. **Cheng Zhang:** Supervision, Project administration, Funding acquisition, Writing – review & editing.

## Declaration of Competing Interest

The authors declare that they have no known competing financial interests or personal relationships that could have appeared to influence the work reported in this paper.

## Acknowledgments

We acknowledge TCGA and GEO databases for providing their platforms and contributors for uploading their meaningful datasets. We also appreciate members in our lab for helpful discussion and technical assistance.

## Supplementary materials

Supplementary material associated with this article can be found, in the online version, at doi:[10.1016/j.tranon.2022.101550](https://doi.org/10.1016/j.tranon.2022.101550).

## References

- U Capitanio, F. Montorsi, Renal cancer, *Lancet* 387 (10021) (2016) 894–906, [https://doi.org/10.1016/S0140-6736\(15\)00046-X](https://doi.org/10.1016/S0140-6736(15)00046-X). Epub 2015/09/01.
- WT Lowrance, EB Elkin, DS Yee, A Feifer, B Ehdia, LM Jacks, et al., Locally advanced prostate cancer: a population-based study of treatment patterns, *BJU Int.* 109 (9) (2012) 1309–1314, <https://doi.org/10.1111/j.1464-410X.2011.10760.x>. Epub 2011/11/17.
- CJ Ricketts, DR Crooks, C Sourbier, LS Schmidt, R Srinivasan, WM. Linehan, Snapshot: renal cell carcinoma, *Cancer Cell* 29 (4) (2016) 610–6e1, <https://doi.org/10.1016/j.ccell.2016.03.021>. Epub 2016/04/14.
- S Turajlic, H Xu, K Litchfield, A Rowan, T Chambers, J Lopez, et al., Tracking cancer evolution reveals constrained routes to metastases: tracerx renal, *Cell* 173 (3) (2018) 581–594, <https://doi.org/10.1016/j.cell.2018.03.057>, e12. Epub 2018/04/17.
- R Torrey, PE Spiess, SK Pal, D. Josephson, Role of surgery for locally advanced and metastatic renal cell carcinoma, *J. Natl. Compr. Canc. Netw.* 9 (9) (2011) 985–993, <https://doi.org/10.6004/jnccn.2011.0083>. Epub 2011/09/16.
- F Massari, A Rizzo, V Mollica, M Rosellini, A Marchetti, A Ardizzoni, et al., Immune-based combinations for the treatment of metastatic renal cell carcinoma: a meta-analysis of randomised clinical trials, *Eur. J. Cancer (Oxford, England: 1990)* 154 (2021) 120–127, <https://doi.org/10.1016/j.ejca.2021.06.015>.
- V Mollica, M Santoni, MR Matrana, U Basso, U De Giorgi, A Rizzo, et al., Concomitant proton pump inhibitors and outcome of patients treated with nivolumab alone or plus ipilimumab for advanced renal cell carcinoma, *Target Oncol.* 17 (1) (2022) 61–68, <https://doi.org/10.1007/s11523-021-00861-y>.
- A Rizzo, V Mollica, M Santoni, AD Ricci, M Rosellini, A Marchetti, et al., Impact of clinicopathological features on survival in patients treated with first-line immune checkpoint inhibitors plus tyrosine kinase inhibitors for renal cell carcinoma: a meta-analysis of randomized clinical trials, *Eur. Urol. Focus* 8 (2) (2022) 514–521, <https://doi.org/10.1016/j.euf.2021.03.001>.
- RJ Deshaies, CA. Joazeiro, Ring Domain E3 Ubiquitin Ligases, *Annu. Rev. Biochem.* 78 (2009) 399–434, <https://doi.org/10.1146/annurev.biochem.78.101807.093809>. Epub 2009/06/06.
- MD Petroski, RJ. Deshaies, Function and Regulation of Cullin-Ring Ubiquitin Ligases, *Nat. Rev. Mol. Cell Biol.* 6 (1) (2005) 9–20, <https://doi.org/10.1038/nrm1547>. Epub 2005/02/03.
- D Frescas, M. Pagano, Deregulation of proteolysis by the F-box proteins Skp2 and Beta-Trep: tipping the scales of cancer, *Nat. Rev. Cancer* 8 (6) (2008) 438–449, <https://doi.org/10.1038/nrc2396>. Epub 2008/05/27.
- C Bai, P Sen, K Hofmann, L Ma, M Goebel, JW Harper, et al., Skp1 Connects Cell Cycle Regulators to the Ubiquitin Proteolysis Machinery through a Novel Motif, the F-Box, *Cell* 86 (2) (1996) 263–274, [https://doi.org/10.1016/S0092-8674\(00\)80098-7](https://doi.org/10.1016/S0092-8674(00)80098-7). Epub 1996/07/26.
- W Shi, L Feng, S Dong, Z Ning, Y Hua, L Liu, et al., Fbxl6 governs C-Myc to promote hepatocellular carcinoma through ubiquitination and stabilization of Hsp90aa1, *Cell Commun Signal* 18 (1) (2020) 100, <https://doi.org/10.1186/s12964-020-00604-y>. Epub 2020/06/25.
- Y Li, K Cui, Q Zhang, X Li, X Lin, Y Tang, et al., Fbxl6 Degrades Phosphorylated P53 to Promote Tumor Growth, *Cell Death Differ.* 28 (7) (2021) 2112–2125, <https://doi.org/10.1038/s41418-021-00739-6>. Epub 2021/02/12.
- G Suske, E Bruford, S. Philippen, Mammalian Sp/Klf transcription factors: bring in the family, *Genomics* 85 (5) (2005) 551–556, <https://doi.org/10.1016/j.ygeno.2005.01.005>. Epub 2005/04/12.
- AR Black, JD Black, J. Azizkhan-Clifford, Sp1 and Kruppel-Like Factor Family of Transcription Factors in Cell Growth Regulation and Cancer, *J. Cell. Physiol.* 188 (2) (2001) 143–160, <https://doi.org/10.1002/jcp.1111>. Epub 2001/06/26.
- WB Yang, PH Chen, Hsu Ts, TF Fu, WC Su, H Liaw, et al., Sp1-mediated microRNA-182 expression regulates lung cancer progression, *Oncotarget* 5 (3) (2014) 740–753, <https://doi.org/10.18632/oncotarget.1608>. Epub 2014/02/13.
- WC Chang, JJ. Hung, Functional role of post-translational modifications of Sp1 in tumorigenesis, *J. Biomed. Sci.* 19 (2012) 94, <https://doi.org/10.1186/1423-0127-19-94>. Epub 2012/11/15.
- H Zhu, S Wang, H Shen, X Zheng, X. Xu, Sp1/Akt/Foxo3 signaling is involved in Mir-362-3p-mediated inhibition of cell-cycle pathway and emt progression in renal cell carcinoma, *Front. Cell Dev. Biol.* 8 (2020) 297, <https://doi.org/10.3389/fcell.2020.00297>. Epub 2020/05/21.
- C Liu, L Liu, K Wang, XF Li, LY Ge, RZ Ma, et al., Vhl-Hif-2alpha Axis-Induced Smyd3 Upregulation Drives Renal Cell Carcinoma Progression Via Direct Trans-Activation of Egrf, *Oncogene* 39 (21) (2020) 4286–4298, <https://doi.org/10.1038/s41388-020-1291-7>. Epub 2020/04/16.
- G Liu, Z Ye, X Zhao, Z Ji, Sp1-induced up-regulation of Lncrna Shhg14 as a Cerna promotes migration and invasion of clear cell renal cell carcinoma by regulating N-Wasp, *Am. J. Cancer Res.* 7 (12) (2017) 2515–2525. Epub 2018/01/10.
- Z Wang, P Liu, H Inuzuka, W. Wei, Roles of F-box proteins in cancer, *Nat. Rev. Cancer* 14 (4) (2014) 233–247, <https://doi.org/10.1038/nrc3700>. Epub 2014/03/25.
- L Yan, M Lin, S Pan, YG Assaraf, ZW Wang, X. Zhu, Emerging roles of F-Box proteins in cancer drug resistance, *Drug Resist. Updat.* 49 (2020), 100673, <https://doi.org/10.1016/j.drug.2019.100673>. Epub 2019/12/27.
- MB Wozniak, F Le Calvez-Kelm, B Abedi-Ardekani, G Byrnes, G Durand, C Carreira, et al., Integrative genome-wide gene expression profiling of clear cell renal cell carcinoma in Czech Republic and in the United States, *PLoS One* 8 (3) (2013) e57886, <https://doi.org/10.1371/journal.pone.0057886>. Epub 2013/03/26.
- PJ Heagerty, T Lumley, MS. Pepe, Time-dependent roc curves for censored survival data and a diagnostic marker, *Biometrics* 56 (2) (2000) 337–344, <https://doi.org/10.1111/j.0006-341x.2000.00337.x>. Epub 2000/07/06.
- KJ Livak, TD. Schmittgen, Analysis of Relative Gene Expression Data Using Real-Time Quantitative Pcr and the 2(-Delta Delta C(T)) Method, *Methods (San Diego, Calif)* 25 (4) (2001) 402–408.
- J Heo, R Eki, T. Abbas, Deregulation of F-box proteins and its consequence on cancer development, progression and metastasis, *Semin. Cancer Biol.* 36 (2016) 33–51, <https://doi.org/10.1016/j.semcancer.2015.09.015>. Epub 2015/10/04.
- A Lanczky, B. Gyorfy, Web-Based Survival Analysis Tool Tailored for Medical Research (KmpLOT): Development and Implementation, *J. Med. Internet Res.* 23 (7) (2021) e27633, <https://doi.org/10.2196/27633>. Epub 2021/07/27.
- F Dang, L Nie, W. Wei, Ubiquitin signaling in cell cycle control and tumorigenesis, *Cell Death Differ.* 28 (2) (2021) 427–438, <https://doi.org/10.1038/s41418-020-00648-0>. Epub 2020/11/02.
- J Cheng, J Guo, Z Wang, BJ North, K Tao, X Dai, et al., Functional Analysis of Cullin 3 E3 Ligases in Tumorigenesis, *Biochim. Biophys. Acta Rev. Cancer* 1869 (1) (2018) 11–28, <https://doi.org/10.1016/j.bbcan.2017.11.001>. Epub 2017/11/13.
- JR Skaar, JK Pagan, M. Pagano, Scf Ubiquitin Ligase-Targeted Therapies, *Nat. Rev. Drug Discov.* 13 (12) (2014) 889–903, <https://doi.org/10.1038/nrd4432>. Epub 2014/11/15.
- J Wu, X Zhang, L Zhang, C-Y Wu, AH Rezaeian, C-H Chan, et al., Skp2 E3 Ligase Integrates Atm Activation and Homologous Recombination Repair by Ubiquitinating Nbs1, *Mol. Cell* 46 (3) (2012) 351–361, <https://doi.org/10.1016/j.molcel.2012.02.018>.
- JJ Miller, MK Summers, DV Hansen, MV Nachury, NL Lehman, A Loktev, et al., Emi1 Stably Binds and Inhibits the Anaphase-Promoting Complex/Cyclosome as a Pseudosubstrate Inhibitor, *Genes Dev.* 20 (17) (2006) 2410–2420.
- DE Nelson, SJ Randle, H. Laman, Beyond Ubiquitination: the atypical functions of Fbxo7 and Other F-Box proteins, *Open Biol.* 3 (10) (2013), 130131, <https://doi.org/10.1098/rsob.130131>.
- F Guo, J Liu, X Han, X Zhang, T Lin, Y Wang, et al., Fbxo22 suppresses metastasis in human renal cell carcinoma via inhibiting Mmp-9-mediated migration and invasion and vegf-mediated angiogenesis, *Int. J. Biol. Sci.* 15 (3) (2019) 647–656, <https://doi.org/10.7150/ijbs.31293>. Epub 2019/02/13.
- Y Cai, M Zhang, X Qiu, B Wang, Y Fu, J Zeng, et al., Upregulation of Fbxw7 suppresses renal cancer metastasis and epithelial mesenchymal transition, *Dis. Markers* 2017 (2017), 8276939, <https://doi.org/10.1155/2017/8276939>. Epub 2017/11/04.
- K Shanmugasundaram, K Block, BK Nayak, CB Livi, MA Venkatachalam, S. Sudarshan, Pi3k Regulation of the Skp-2/P27 Axis through Mtorc2, *Oncogene* 32 (16) (2013) 2027–2036, <https://doi.org/10.1038/onc.2012.226>. Epub 2012/06/27.
- M Seifi-Alan, R Shamsi, S Ghafouri-Fard, R Mirfakhraie, D Zare-Abdollahi, A Movafagh, et al., Expression Analysis of Two Cancer-Testis Genes, Fbxo39 and Tdrd4, in Breast Cancer Tissues and Cell Lines, *Asian Pac. J. Cancer Prev.* 14 (11) (2014) 6625–6629, <https://doi.org/10.7314/apjcp.2013.14.11.6625>. Epub 2014/01/01.
- YC Liu, S Yan, DM Liu, DX Pei, YW. Li, Aberrant expression of cancer-testis antigen Fbxo39 in breast cancer and its clinical significance, *Clin. Lab.* 66 (9) (2020), <https://doi.org/10.7754/Clin.Lab.2020.200121>. Epub 2020/09/10.
- C Bai, R Richman, SJ. Elledge, Human Cyclin F, *EMBO J.* 13 (24) (1994) 6087–6098. Epub 1994/12/15.
- R Choudhury, T Bonacci, A Arceci, D Lahiri, CA Mills, JL Kernan, et al., Apc/C and Scf(Cyclin F) constitute a reciprocal feedback circuit controlling S-phase entry, *Cell Rep.* 16 (12) (2016) 3359–3372, <https://doi.org/10.1016/j.celrep.2016.08.058>. Epub 2016/09/23.
- MJ Emanuele, TP Enrico, RD Mouery, D Wasserman, S Nachum, A. Tzur, Complex Cartography: Regulation of E2f Transcription Factors by Cyclin F and Ubiquitin, *Trends Cell Biol.* 30 (8) (2020) 640–652, <https://doi.org/10.1016/j.tcb.2020.05.002>. Epub 2020/06/10.
- TP Enrico, W Stallaert, ET Wick, P Ngoi, X Wang, SM Rubin, et al., Cyclin F drives proliferation through Scf-dependent degradation of the retinoblastoma-like tumor suppressor P130/Rb2, *Elife* 10 (2021), <https://doi.org/10.7554/eLife.70691>. Epub 2021/12/02.
- M Morel, KN Shah, W. Long, The F-box protein Fbxl16 up-regulates the stability of C-Myc oncoprotein by antagonizing the activity of the F-Box protein Fbw7, *J. Biol. Chem.* 295 (23) (2020) 7970–7980, <https://doi.org/10.1074/jbc.RA120.012658>. Epub 2020/04/30.
- YJ Kim, Y Zhao, JK Myung, JM Yi, MJ Kim, SJ. Lee, Suppression of breast cancer progression by Fbxl16 via oxygen-independent regulation of Hif1alpha stability, *Cell Rep.* 37 (8) (2021), 109996, <https://doi.org/10.1016/j.celrep.2021.109996>. Epub 2021/11/25.